OPEN

Citation: Cell Death and Disease (2014) 5, e1269; doi:10.1038/cddis.2014.218

www.nature.com/cddis

Mammalian STE20-like kinase 2, not kinase 1, mediates photoreceptor cell death during retinal detachment

H Matsumoto[1], Y Murakami[1], K Kataoka[1], H Lin[1], KM Connor[1], JW Miller[1], D Zhou[2], J Avruch[3] and DG Vavvas*,[1]

Photoreceptor cell death is the definitive cause of vision loss in retinal detachment (RD). Mammalian STE20-like kinase (MST) is a master regulator of both cell death and proliferation and a critical factor in development and tumorigenesis. However, to date the role of MST in neurodegeneration has not been fully explored. Utilizing MST1$^{-/-}$ and MST2$^{-/-}$ mice we identified MST2, but not MST1, as a regulator of photoreceptor cell death in a mouse model of RD. MST2$^{-/-}$ mice demonstrated significantly decreased photoreceptor cell death and outer nuclear layer (ONL) thinning after RD. Additionally, caspase-3 activation was attenuated in MST2$^{-/-}$ mice compared to control mice after RD. The transcription of p53 upregulated modulator of apoptosis (PUMA) and Fas was also reduced in MST2$^{-/-}$ mice post-RD. Retinas of MST2$^{-/-}$ mice displayed suppressed nuclear relocalization of phosphorylated YAP after RD. Consistent with the reduction of photoreceptor cell death, MST2$^{-/-}$ mice showed decreased levels of proinflammatory cytokines such as monocyte chemoattractant protein 1 and interleukin 6 as well as attenuated inflammatory CD11b cell infiltration during the early phase of RD. These results identify MST2, not MST1, as a critical regulator of caspase-mediated photoreceptor cell death in the detached retina and indicate its potential as a future neuroprotection target.

Cell Death and Disease (2014) **5,** e1269; doi:10.1038/cddis.2014.218; published online 29 May 2014
Subject Category: Neuroscience

Retinal detachment (RD) occurs when the photoreceptors of the retina become separated from the underlying retinal pigment epithelium. RD causes photoreceptor cell death, which leads to visual decline. The primary cause of photoreceptor cell death in response to RD is apoptosis,[1] and Fas signaling is a major cell death pathway activated in the detached retina.[1–4] Several retinal disorders are associated with RD including age-related macular degeneration,[5] diabetic retinopathy,[6] retinopathy of prematurity,[7] as well as rhegmatogenous RD.[8] Medical and surgical treatments for these diseases have been improved over recent years. However, visual acuity is not always restored after successful reattachments due to the induction of photoreceptor cell death that resulted from the RD. Only two-fifths of patients with rhegmatogenous RD involving the macula, a region essential for central vision, recover 20/40 or better vision.[9,10] Therefore, identification of the mechanisms involved in photoreceptor cell death after RD is critical to developing new treatment strategies with the aim of preserving photoreceptor cell viability.

The Mammalian Sterile 20-like kinase (MST) 1/2 are homologs of *Drosophila* Hippo kinase.[11] The Hippo pathway has been shown to have a critical role in controlling organ size by regulating both cell proliferation and apoptosis.[12–16] Upon activation of mammalian Hippo pathway, MST1/2 form protein complex involving Salvador (SAV) 1, large tumor suppressor (LATS) 1/2 and Mps one binder (MOB) 1, which phosphorylates and inactivates Yes-associated protein (YAP).[17–19] YAP is a transcriptional coactivator, which binds to a nuclear-localized transcription factor TEA domain family (TEAD) and potentiates the cells proliferative and anti-apoptotic pathways.[20,21] Mutations in the Hippo pathway increase the levels of functional YAP in the nucleus, which leads to the sustained proliferating and anti-apoptotic transcriptional programs and overcomes organ size control to promote cancer development.[22–26] It has been reported that phosphorylated YAP binds to 14-3-3 in cytoplasm, which leads to cytoplasmic retention of phosphorylated YAP.[17,18] However, recent studies revealed that phosphorylated YAP also relocalizes into nucleus and binds to a transcription factor p73, which exerts apoptotic activity.[27–30] Therefore, Hippo pathway controls both cell proliferation and death through the modulation in cellular localization of YAP and phosphorylated YAP. Although the upstream regulators of mammalian Hippo pathway have not been clarified, several studies have reported that Fas active receptor promoted the initiation of the mammalian Hippo pathway.[28,31–33]

MST1/2 have recently been suggested to mediate neuronal cell death.[34–37] However, their precise roles in various neurodegenerations have not been fully elucidated. In this study, we induced experimental RD in mice deficient in MST1 or MST2 in order to investigate the role of mammalian Hippo pathway in RD-induced photoreceptor cell death.[38] Our results indicate that MST2, not MST1, plays a critical role in photoreceptor cell death in the detached retina.

[1]Retina Service, Angiogenesis Laboratory, Massachusetts Eye and Ear Infirmary, Department of Ophthalmology, Harvard Medical School, Boston, MA 02114, USA; [2]State Key Laboratory of Stress Cell Biology, School of Life Sciences, Xiamen University, Xiamen, Fujian 361102, China and [3]Department of Molecular Biology, Massachusetts General Hospital, Boston, MA 02114, USA
*Corresponding author: DG Vavvas, Retina Service, Angiogenesis Laboratory, Massachusetts Eye and Ear Infirmary, Department of Ophthalmology, Harvard Medical School, 325 Cambridge Street, Boston, MA 02114, USA. Tel: +1 617 573 6874; Fax: +1 617 573 3011; E-mail vavvas@meei.harvard.edu
Keywords: retinal detachment photoreceptor cell; apoptosis; neurodegeneration; mammalian STE20-like kinase
Abbreviations: RD, retinal detachment; MST, mammalian STE20-like kinase
Received 18.3.14; accepted 14.4.14; Edited by N Bazan

Results

Expression of MST1/2 mRNA and protein in the retina. MST1 and MST2 are ubiquitously expressed serine/threonine kinases. We first assessed if the loss of MST1 or MST2 led to upregulation of the corresponding MST protein by WB using the whole retinas of mice without RD. MST1$^{-/-}$ or MST2$^{-/-}$ mice showed no upregulation of MST2 or MST1 protein, respectively. (Figures 1a and b). Next, we checked *MST1* and *MST2* mRNA expressions in photoreceptor cells by laser capture microdissection (LCM) and reverse transcriptional PCR. Complementary DNA (cDNA) from whole retina of MST1$^{-/-}$ or MST2$^{-/-}$ mouse was used as a negative control. Both *MST1* and *MST2* mRNAs were expressed in outer nuclear layer (ONL), which consists of photoreceptor cell nuclei (Figures 1c and d). Given the role of Hippo pathway in organ development and tumorigenesis, we wanted to assess if any morphologic changes occurred within the retina when MST1 or MST2 was knocked out. Histological examination showed that the absence of MST1 or MST2 protein did not result in any obvious morphologic state under normal conditions (Figures 1e and f).

MST2 deficiency rescues photoreceptors from RD-induced cell death. Given the role of the Hippo pathway in apoptosis, we investigated the function of MST1 and 2 proteins in our experimental mouse RD model, which results in the death of photoreceptor cells that compromise the ONL. Our RD model shows the peak of TUNEL (TdT-dUTP terminal nick-end labeling)-positive cells on day 1. Therefore, we analyzed TUNEL-positive cell density in ONL at 12 h, 1, 3, 5 and 7 days after RD (Figures 2a–d). Reduction in ONL thickness was assessed as ONL/INL (inner nuclear layer) ratio on day 7 (Figures 2e and f). MST1$^{-/-}$ mice had no significant differences in TUNEL-positive cell density and ONL thickness compared with control mice (Figures 2c and e). In contrast, MST2$^{-/-}$ mice demonstrated significantly less photoreceptor cell death than WT mice at 12 h (WT: 1015 ± 199 cells/mm^2 and MST2$^{-/-}$: 376 ± 70 cells/mm^2; $P = 0.009$), 24 h (WT: 1833 ± 165 cells/mm^2 and MST2$^{-/-}$: 516 ± 126 cells/mm^2; $P = 0.0001$), and 72 h (WT: 628 ± 74 cells/mm^2 and MST2$^{-/-}$: 294 ± 25 cells/mm^2; $P = 0.008$) after RD (Figure 2d). Moreover, MST2$^{-/-}$ mice displayed significantly higher ONL/INL ratio than control mice (WT: 1.65 ± 0.04 and MST2$^{-/-}$: 1.83 ± 0.04; $P = 0.017$; Figure 2f). These results indicate that MST2 plays a critical role in initiating RD-induced photoreceptor cell death.

MST2 deficiency attenuates cell death signaling after RD. The final step of MST pathway is phosphorylation of

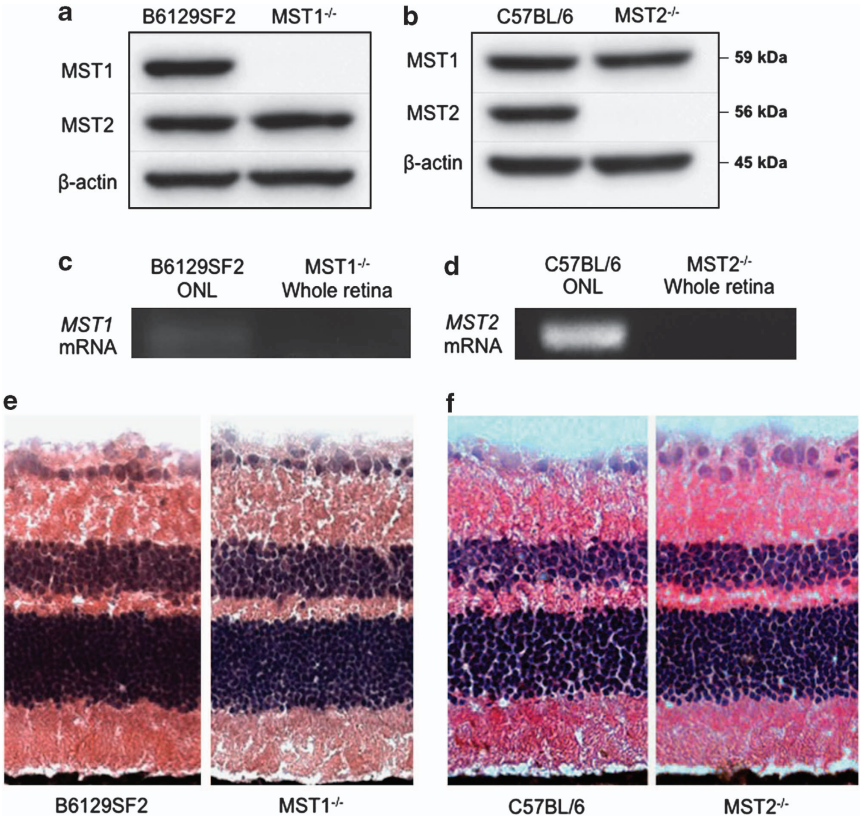

Figure 1 MST1 and MST2 expressions in the retina. (**a** and **b**) Western blot analysis for MST1 and MST2 in the retina. MST1 or MST2 protein is deleted in MST1$^{-/-}$ or MST2$^{-/-}$ mice, respectively. Both strains show no upregulation of the corresponding MST proteins. (**c** and **d**) Reverse transcriptional PCR for MST1 (**c**) or MST2 (**d**) in outer nuclear layer. MST1$^{-/-}$ or MST2$^{-/-}$ whole retina was used as a negative control. MST1 or MST2 mRNA is expressed in photoreceptor cells in B6129SF2 or C57BL/6 mice, respectively. (**e** and **f**) Retinal histology of untreated B6129F2 and MST1$^{-/-}$ mice (**e**), or C57BL/6 and MST2$^{-/-}$ mice (**f**). MST1$^{-/-}$ and MST2$^{-/-}$ mice display normal phenotype

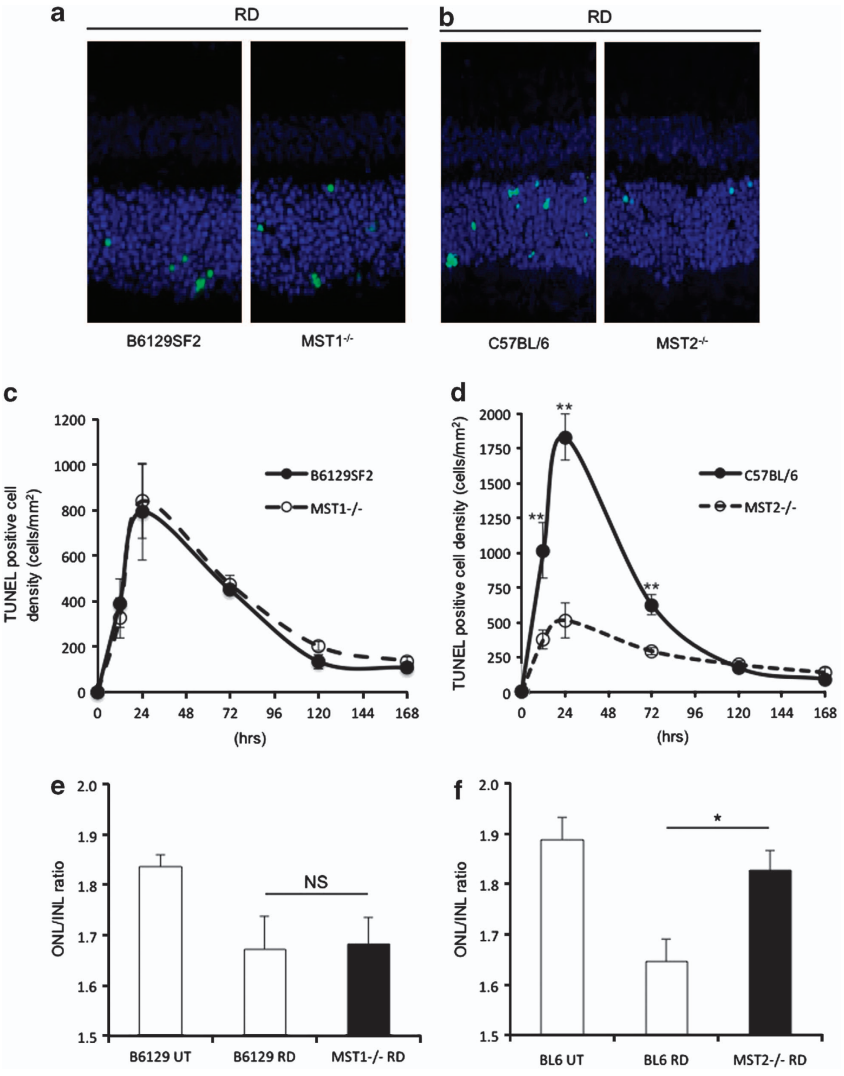

Figure 2 MST2, but not MST1, mediates photoreceptor cell death after RD. (**a**–**d**) TUNEL (green) and TO-PRO-3 (blue) staining at 24 h after RD (**a** and **b**) and time course of TUNEL-positive cell density in outer nuclear layer (ONL; $n = 6$ each group and time point, **c** and **d**). There were no significant differences between B6129SF2 and MST1$^{-/-}$ mice at any time points (**c**). Conversely, MST2$^{-/-}$ mice displayed significantly less photoreceptor cell death than C57BL/6 mice 12, 24, 72 h after RD (**$P < 0.01$ each, **d**). (**e** and **f**) ONL/INL (inner nuclear layer) ratio 7 days after RD ($n = 6$ each). There was no significant difference between B6129SF2 and MST1$^{-/-}$ mice (**e**). On the other hand, MST2$^{-/-}$ mice showed significantly higher ONL/INL ratio than C57BL/6 mice (*$P < 0.05$) (**f**). The graphs show mean ± S.E.M.

YAP. It is generally believed that phosphorylated YAP binds to 14-3-3 leading to cytoplasmic retention, which decreases YAP nuclear localization and YAP/TEAD transcriptional activity.[17–19] However, recent studies reported that phosphorylated YAP might be able to relocalize into nucleus and bind to p73 in the cell undergoing cell death.[27–30] To evaluate the nuclear localization of phosphorylated YAP after RD, we performed nuclear extraction followed by WB using the whole retina at 24 h after RD. MST2$^{-/-}$ mice showed less phosphorylated YAP in the nucleus compared with WT mice (Figure 3a). We further assessed the binding between phosphorylated YAP and p73 as well as between YAP and TEAD after RD by immunoprecipitation and subsequent WB analysis (Supplementary Figure S1). Consistent with the nuclear localization of phosphorylated YAP, MST2$^{-/-}$ mice displayed less p73 binding phosphorylated YAP than WT mice. Unexpectedly, TEAD binding YAP was also less in MST2$^{-/-}$ than WT mice, which might reflect the fewer proliferating cells in the detached retina such as microglia in MST2$^{-/-}$ mice.

p73 has been reported to induce transcriptional upregulation of p53 upregulated modulator of apoptosis (PUMA), which in turn provokes BAX mitochondrial translocation and cytochrome *c* release.[28,39] Moreover, a previous study revealed that p73 activation induces upregulation of Fas transcription and expression at cell surface.[40] On the other hand, YAP activation was reported to induce a high expression of cIAP1 and Survivin, members of the inhibitor of apoptosis protein (IAP) family.[22,41,42] Thus we evaluated PUMA and Fas as well as cIAP1 and Survivin gene transcriptions at 24 h after RD. Consistent with the results of immunoprecipitation, MST2$^{-/-}$ mice showed significantly less *PUMA* (45% of WT, $P = 0.009$) and *Fas* (64% of WT, $P = 0.026$) mRNA expression after RD compared with WT

mice, whereas there were reduction trends that did not reach statistical significant differences in *cIAP1* and *Survivin* mRNA expressions in MST2$^{-/-}$ mice (Figures 3b–e), indicating that phosphorylated YAP/p73-mediated cell death signaling is substantially attenuated in MST2$^{-/-}$ mice.

Finally, we assessed cleaved caspase-3 protein expression at 24 h after RD. Cleaved caspase-3 is one of effector caspases, which is the downstream of Fas receptor—mediated apoptotic pathway and mitochondrial apoptotic pathway.[2] In accordance with our expectation, cleaved caspase-3 protein level in MST2$^{-/-}$ mice after RD was significantly decreased compared with that of WT mice ($P=0.011$; Figure 3f), suggesting that MST2 mediates caspase-dependent photoreceptor apoptosis in the detached retina.

Reduced proinflammatory cytokine generation and macrophage infiltration in MST2$^{-/-}$ mice after RD. We previously described that monocyte chemoattractant protein 1 (MCP-1) is an essential mediator of early infiltration of

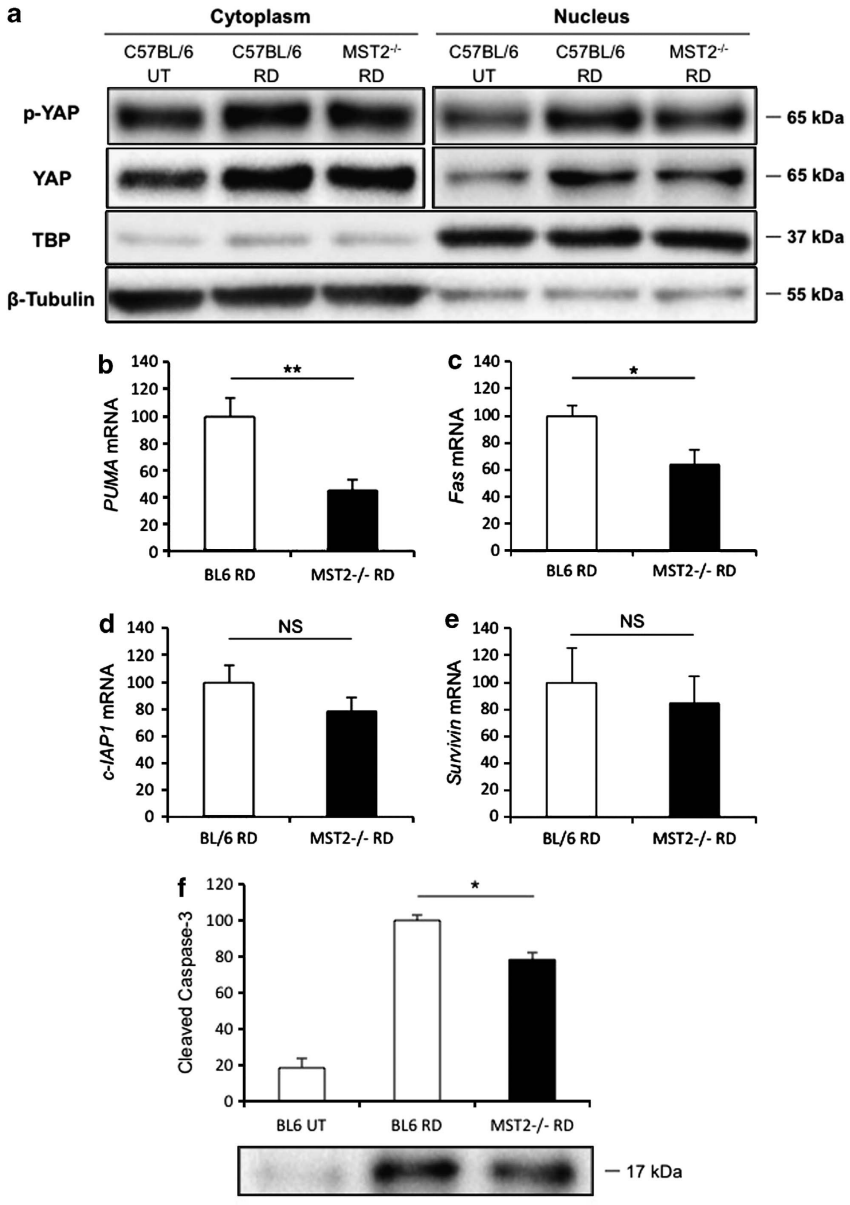

Figure 3 MST2 promotes nuclear relocalization of phosphorylated YAP and mediates apoptosis signaling after RD. (**a**) Western blot analysis for phosphorylated YAP and total YAP in the retina at 24 h after RD using nuclear and cytoplasmic fractions. MST2$^{-/-}$ mice displayed less nuclear localization of phosphorylated YAP as well as total YAP than WT mice after RD. TBP and β-tubulin were monitored as markers for the purity of the nuclear and cytoplasmic fractions, respectively. Representative images from three independent experiments are shown. (**b**–**e**) Quantitative real-time PCR analysis for PUMA (**b**), Fas (**c**), cIAP1 (**d**) and Survivin (**e**) in the retina at 24 h after RD ($n=6$ each). MST2$^{-/-}$ mice showed significantly less *PUMA* (**$P<0.01$) and *Fas* (*$P<0.05$) mRNA expression than WT mice, whereas there were no significant differences in *cIAP1* and *Survivin* mRNA expressions. (**f**) Western blot analysis for cleaved caspase-3 in the retina at 24 h after RD ($n=6$ each). MST2$^{-/-}$ mice displayed significantly less cleaved caspase-3 than WT mice (**$P<0.05$). The bar graphs indicate the relative level of cleaved caspase-3 to β-actin by densitometric analysis. Each sample for western blot analysis includes at least six retinas. Bl.6 = Wild type (WT). The graphs show mean ± S.E.M.

macrophage/microglia after RD.[43] Zacks *et al*.[44] described that interleukin 6 (IL-6) is increased after RD using gene microarray analysis.[44] IL-6 is a pleiotropic cytokine with a role in inflammation as well as hematopoiesis, angiogenesis, cell differentiation and neuronal survival. Thus, we evaluated MCP-1 and IL-6 expression levels by enzyme-linked immunosorbent assay (ELISA). MST2$^{-/-}$ mice demonstrated significantly less MCP-1 (WT: 253 ± 18 pg/mg and MST2$^{-/-}$: 194 ± 2 pg/mg; $P = 0.035$) and IL-6 (WT: 21.3 ± 2.2 pg/mg and MST2$^{-/-}$: 12.6 ± 0.9 pg/mg; $P = 0.014$) levels than WT mice at 24 h after RD. MCP-1 and IL-6 levels were rapidly decreased after day 1 in both groups (Figures 4a and b). We next analyzed the inflammatory reaction by immunofluorescence detection of the macrophage/microglial marker CD11b. MST2$^{-/-}$ mice showed significantly less CD11b-positive cell density than WT mice at 24 h after RD (WT: 161 ± 17 cells/mm^2 and MST2$^{-/-}$: 85 ± 9 cells/mm^2; $P = 0.007$). WT mice kept the CD11b-positive cell density after day 1, whereas that in MST2$^{-/-}$ mice was increased to the same level as WT mice 3 days after RD (Figures 4c and d). These results indicate that MST2 mediates the inflammation during the early phase of RD.

Discussion

MST1/2 are ubiquitously expressed and known for their function in promoting cell death. MST is critical for organ development and tumorigenesis suppression.[12–16,22–26] Recently, mammalian Hippo pathway has been implicated in playing a role in neurodegeneration,[34–37] however, the functional differences between MST1 and MST2 in various neurodegenerations have not been well explored. Thus, we investigated the role of MST1/2 in photoreceptor cell death using a mouse RD model. We induced RD in mice deficient in MST1 or MST2 and evaluated photoreceptor cell death. In contrast to Lee *et al*.[37] MST1 deletion had no effect on RD-induced neuronal cell death, whereas MST2 deletion significantly attenuated photoreceptor cell death after RD (Figure 2) and subsequent inflammatory response including MCP-1 and IL-6 secretion as well as CD11b-positive cell infiltration (Figure 4). Therefore, we define the involvement of MST2, but not MST1, as a regulator of photoreceptor cell death after RD. Both MST1$^{-/-}$ and MST2$^{-/-}$ mice show normal retinal phenotype (Figures 1e and f), suggesting that single deficiency of MST1 or MST2 does not affect the normal retinal development.

Upon activation, MST1/2 form protein complex involving SAV1, LATS1/2 and MOB1, which phosphorylates YAP. It is generally believed that phosphorylated YAP binds to 14-3-3 leading to cytoplasmic retention, which decreases YAP/TEAD nuclear complex and its transcriptional activity.[17–19] However, recently, several investigators reported that phosphorylated YAP might be able to relocalize into nucleus and bind to p73 under cell death stimulations and potentiate p73 apoptotic activity.[27–30] Accumulating evidences also indicate that Fas signaling may modulate the activity of mammalian Hippo pathway. Moreover, Fas signaling is well known to be involved in photoreceptor cell death after RD.[1–4] Consistent with these reports, nuclear localization of phosphorylated YAP after RD was suppressed in MST2$^{-/-}$ mice in the current study (Figure 3a). Furthermore, p73 binding phosphorylated YAP was reduced in MST2$^{-/-}$ mice after RD (Supplementary Figure S1). These results indicate that MST2 plays a critical role in nuclear relocalization of phosphorylated YAP and subsequent p73 binding after RD.

Matallanas *et al*.[28] reported that p73–YAP1 complex directly enhanced transcription of *PUMA* gene. Consistent with this report, *PUMA* mRNA expression was significantly attenuated in MST2$^{-/-}$ mice after RD (Figure 3b). PUMA is a Bcl-2 family member/BH3-only protein, which exists in the cytosol in unstressed cells and accumulates onto the mitochondrial membrane upon death stimuli. PUMA mediates Bax (Bcl-2 family member/Bax subfamily) translocation from cytosol into mitochondria, thus leading to cytochrome *c* release and caspase activation.[39] p73 activation is also reported to induce upregulation of Fas transcription and expression at cell surface.[40] In accordance with this report, *Fas* mRNA expression was significantly suppressed in MST2$^{-/-}$ mice after RD (Figure 3b). Fas is one of death receptors, which mediates mainly apoptotic signaling. Fas signaling will increase cleaved caspase-3 level through receptor-mediated apoptotic pathway as well as mitochondrial apoptotic pathway.[2] Moreover, increased Fas signaling will enhance the activation of mammalian Hippo pathway, which might result in the positive feedback loop. As expected from reduced *PUMA* and *Fas* mRNA expression, MST2$^{-/-}$ mice showed significantly lower cleaved caspase-3 protein expression compared with WT mice after RD (Figure 3f). Taken together, our data indicate MST2 mediates RD-induced photoreceptor cell death in caspase-dependent manner.

We expected that WT mice would show less TEAD binding YAP than MST2$^{-/-}$ mice after RD, because YAP is reported to translocate from nucleus to cytoplasm under the activation of mammalian Hippo pathway. However, TEAD binding YAP was elevated in WT mice compared with MST2$^{-/-}$ mice (Supplementary Figure S1), whereas there were reduction trends that did not reach statistical significant differences in *cIAP1* and *Survivin* mRNA expressions (Figures 3d and e), which are reported to increase under YAP activation. It has been known that several types of retinal cells including microglia, Müller cell and astrocyte, proliferate after RD,[45–49] in which YAP might be activated and mediate proliferative and anti-apoptotic signaling. In the current study, microglial proliferation in the detached retina was more marked in WT than MST2$^{-/-}$ mice 24 h after RD (Figures 4c and d). This might result in the higher YAP/TEAD binding in WT mice because whole retina was used for the immunoprecipitation assay.

In contrast to MST2$^{-/-}$ mice, MST1$^{-/-}$ mice showed no protective effect on photoreceptor cell death after RD in this study (Figure 2). MST2 shares 98% identity with MST1 in the catalytic domain, but only 60% in the regulatory region.[50] It also shares more homology than MST1 with Hippo.[51] Moreover, MST1/2 expression profile depends on the cell type.[52] Although both MST1 and MST2 are ubiquitously expressed, these differences might lead to the functional difference between MST1 and MST2 in photoreceptor cell death after RD. Fas signaling is reported to activate MST2 via activation of Ras-association domain family 1 and subsequent inhibition of rapidly accelerated fibrosarcoma (RAF) 1.[28] Proteomic

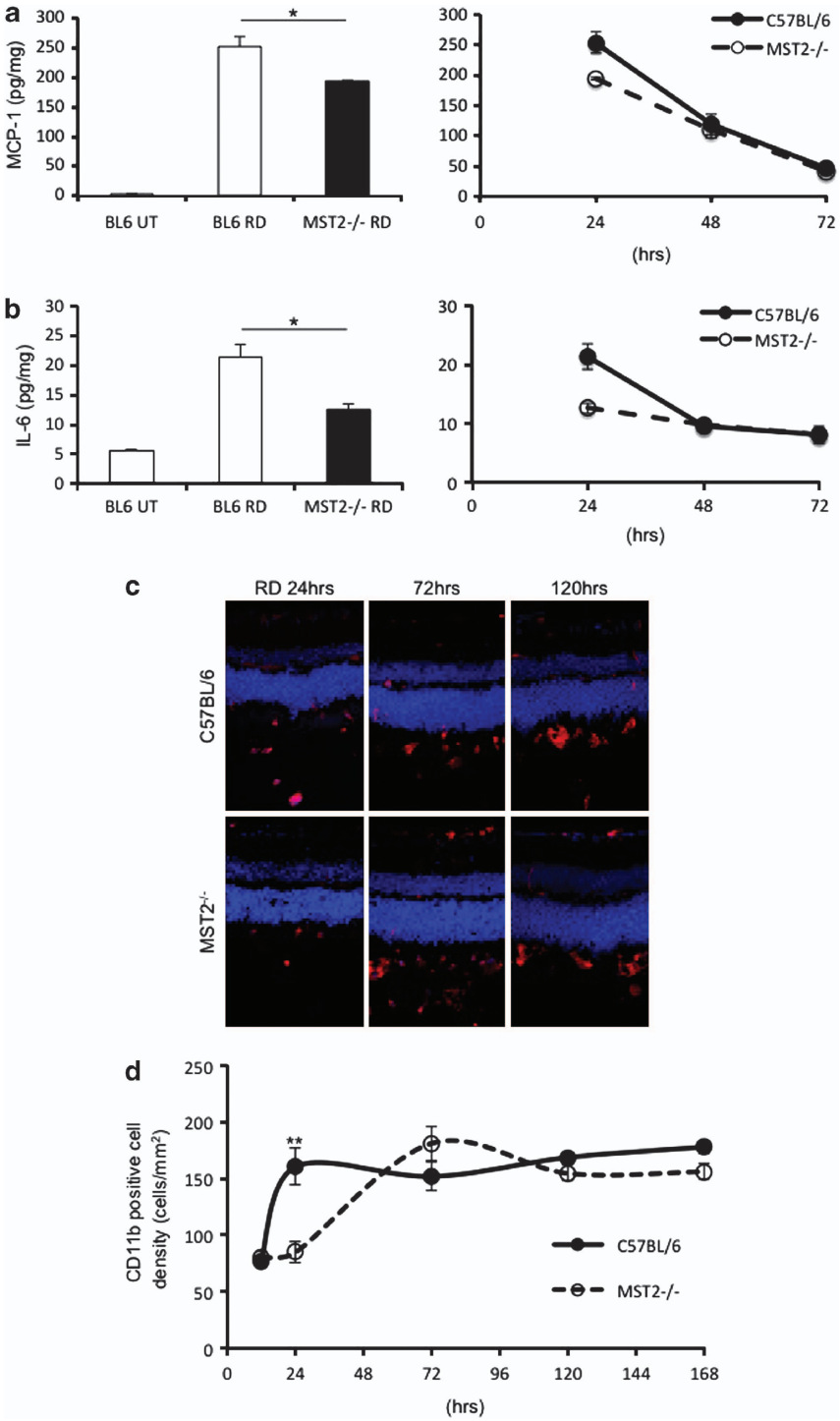

Figure 4 MST2 promotes inflammatory response after RD. (**a** and **b**) ELISA to detect MCP-1 (**a**) and IL-6 (**b**) in the WT and MST2$^{-/-}$ retinas at 24, 48, 72 h after RD ($n=8$ each). MCP-1 and IL-6 generation at 24 h after RD was suppressed in MST2$^{-/-}$ mice (*$P<0.05$). After day 1, MCP-1 and IL-6 levels were decreased in both groups. (**c** and **d**) Immunofluorescence for CD11b (**c**) and time course of CD11b-positive cell density (**d**) in WT and MST2$^{-/-}$ mice ($n=6$ each group and time point). Infiltration of CD11b-positive cells was substantially decreased in MST2$^{-/-}$ mice at 24 h after RD (**$P<0.01$). WT mice kept the CD11b-positive cell density after day 1, whereas that in MST2$^{-/-}$ mice was increased to the same level as WT mice 3 days after RD. The graphs show mean ± S.E.M.

studies have identified several protein kinases that coprecipitate with RAF1 including MST2 but not MST1.[53–56] This can be an explanation for the difference in protective effect on photoreceptor cell death after RD between MST1$^{-/-}$ and MST2$^{-/-}$ mice. In contrast with our results, Lee *et al.*[37] recently reported that MST1 mediates neurodegeneration in a mouse model of amyotrophic lateral sclerosis (ALS).[37] This difference may relate to the cell type involved (photoreceptors

versus motor neurons) and/or the triggers of neuronal cell death. They described that MST1 modulates oxidative stress-initiated neurodegeneration. Oxidative stress is also one of important triggers in photoreceptor cell death after RD,[1,57,58] however the intensity and duration of the oxidative stress may differ when compared to the ALS model.

We previously reported that MCP-1 is an essential mediator of early infiltration of macrophage/microglia after RD.[43] In accordance with this, MST2$^{-/-}$ mice, whose photoreceptor cell death and MCP-1 levels were significantly lower than those of WT mice, showed significantly less CD11b-positive cell density at 24 h after RD. However, MCP-1 and IL-6 levels were decreased after day 1, whereas CD11b-positive cell density was kept at high level in the late phase of RD in both groups (Figure 4). These results indicate that other chemotactic factors might be involved in the late phase of macrophage/microglia infiltration. In addition, recent studies disclosed that macrophage is divided into two types (M1/M2) depending on its function.[59–61] The M1 macrophages express high levels of proinflammatory cytokines, and produce reactive nitrogen and oxygen intermediates. In contrast, M2 macrophages have immunoregulatory functions and promote tissue remodeling. They are also characterized by efficient phagocytic activity and high expression of scavenging molecules. It is possible that the macrophage/microglia in the early and the late phase of RD might be of different class.

Necrotic photoreceptor cell death is known to occur after RD and other retinal photoreceptor degenerations, although its frequency is approximately half that of apoptosis.[1,62] It has been reported that necrotic cells release damage-associated molecular patterns (DAMPs) and enhance inflammatory response.[63–65] DAMPs activate macrophages as Toll-like receptor ligands. The activated macrophages then release inflammatory cytokines such as IL-1, 6 and 8.[66,67] In the current study, IL-6 level was consistent with photoreceptor cell death and CD11b-positive cell density at 24 h after RD, suggesting that IL-6 might be derived mainly from DAMPs activated macrophages.

In conclusion, we investigated the role of mammalian Hippo pathway in neurodegeneration using a mouse RD model. In contrast to prior reports in neurodegenration, MST1 did not appear to play a role in photoreceptor degeneration after RD. However, MST2 was identified as a critical mediator in RD-induced photoreceptor cell death. Blockade of MST2 may suppress photoreceptor cell death and dampen early inflammation, suggesting that MST2 may be a potential target for retinal degenerative diseases associated with RD and inflammation.

Materials and Methods

Animals. All animal experiments followed the guidelines of the ARVO Statement for the Use of Animals in Ophthalmic and Vision Research, and the protocols were approved by the Animal Care Committee of the Massachusetts Eye and Ear Infirmary. We generated MST1$^{-/-}$ and MST2$^{-/-}$ mice and their details were described previously.[24] The background of MST1$^{-/-}$ or MST2$^{-/-}$ mouse used in this study is B6129 or C57BL/6 mouse, respectively. Age- and gender-matched B6129SF2 or C57BL/6 mice were purchased from Jackson Laboratories (Bar Harbor, ME, USA) or Charles River Laboratories (Wilmington, MA, USA), respectively. Mice were fed standard laboratory chow and allowed free access to water in an air-conditioned room with a 12-h light/12-h dark cycle. All mice were used at postnatal 8 ± 1 weeks.

Creation of RD. We modified a previously reported method for creating RDs and created bullous and persistent RDs.[38] Briefly, mice were anesthetized with an intraperitoneal injection of a mixture of 60 mg/kg ketamine and 6 mg/kg xylazine, and pupils were dilated with topical phenylephrine (5%) and tropicamide (0.5%). The temporal conjunctiva at the posterior limbus was incised and detached from the sclera. A 30-gauge needle (BD, Franklin Lakes, NJ, USA) was used with the bevel pointed up to create a sclerotomy 1 mm posterior to the limbus. A scleral tunnel was created followed by scleral penetration into the choroid, which makes a self-sealing scleral wound. A corneal puncture was made with a 30-gauge needle to lower intraocular pressure. Then a 34-gauge needle connected to a 10-μl syringe (NanoFil 10 μl syringe; WPI, Sarasota, FL, USA) with the bevel pointed down was inserted into the subretinal space and 4 μl of 1% sodium hyaluronate (Provisc; Alcon, Fort Worth, TX, USA) was injected gently to detach the neurosensory retina from the underlying RPE. Approximately 60% of the temporal-nasal neurosensory retina was detached. Finally, cyanoacrylate surgical glue (Webglue; Patterson Veterinary, Devens, MA, USA) was put on the scleral wound and the conjunctiva was reattached to the original position. Any eyes with subretinal hemorrhage were excluded from the study.

TUNEL. Following RD, eyes were enucleated at multiple time points and embedded in OCT compound (Tissue Tek; Sakura Finetec, Torrance, CA, USA). Serial sections of the eyes in the sagittal plane were cut at 10 μm thickness on a cryostat (CM1850; Leica, Heidelberg, Nussloch, Germany) at $-20\,^{\circ}$C and prepared for staining. TUNEL assay was performed according to the manufacturer's protocol (ApoTag Fluorescein In Situ Apoptosis Detection Kit; Millipore, Billerica, MA, USA). Finally, sections were counterstained with TO-PRO-3. The number of TUNEL-positive cells was counted in the photoreceptor cell layer (ONL). The area of ONL was also measured by Image J software (developed by Wayne Rasband, National Institutes of Health, Bethesda, MD, USA; available at http://rsb.info.nih.gov/ij/index.html), and then TUNEL-positive cell density in ONL was calculated. A preliminary experiment revealed that the center of RD had less variability of TUNEL-positive cell density (data not shown). Thus subsequent analysis was performed using sections around 1000 μm from the injection site. The average of the TUNEL-positive cell density from two separate locations of each section (see Supplementary Figure S2) was calculated as the representative TUNEL-positive photoreceptor cell density of the section. Then, the average of the TUNEL-positive photoreceptor cell densities from three sections was figured as the representative TUNEL-positive photoreceptor cell density of the eye. Photographs were taken by confocal microscopy using a HCX APOL 40 $\times$ lens (Leica, Allendale, NJ, USA).

Evaluation of ONL/INL ratio. The ONL and INL areas of the detached retina were measured by Image J software and ONL/INL ratio was calculated. Areas of abnormal retinal morphology were excluded so that uniform unbiased measurements can be obtained.

Western blot analysis. Whole retina from untreated or RD-induced eye was dissected from the RPE choroid. Total retinal lysate was used to evaluate MST1, MST2 and cleaved caspase-3 expressions. Nuclear and cytoplasmic extraction was performed according to the manufacturer's protocol (Nuclear Extract Kit; Active Motif North America, Carlsbad, CA, USA) to assess nuclear YAP and phosphorylated YAP expression. At least six retinas were used for each sample. Samples were run on 4–12% Bis-Tris gel (NuPAGE; Invitrogen, Camarillo, CA, USA) electrophoresis and transferred onto PVDF membranes (0.45 μm pores; Millipore, Billerica, MA, USA). After blocking with 3% nonfat dried milk, the membranes were incubated overnight with primary antibody (MST1, YAP, phosphorylated YAP, Cleaved Caspase-3, β-actin, β-tubulin: 1:1000 (Cell Signaling, Danvers, MA, USA), MST2: 1:10 000, TBP: 1:2000 (Abcam, Cambridge, MA, USA)). The blotted membranes were then incubated for 30 min at room temperature with HRP-labeled secondary antibody. Immunoreactive bands were visualized by ECL and detected by ChemiDoc MP Imaging System (Hercules, CA, USA).

Immunoprecipitation. Equal amount of retinal lysates (1 mg) were incubated with 25 μg of protein A agarose beads (Cell Signaling) for 1 h to remove non-specific protein binding. The supernatants were then incubated with 3 μg anti-p73 antibody (Santa Cruz Biotechnology, Santa Cruz, CA, USA) or 5 μg anti-TEF-1 antibody (BD Biosciences, San Jose, CA, USA) for 2 h, followed by incubation with 25 μg of protein A agarose for 3 h. Each incubation was done at 4 $^{\circ}$C. Beads were washed five times with lysis buffer and the immunopellets were then subjected to western blotting.

LCM. Eyes from control mice were embedded in OCT compound immediately after enucleation, cut into 30-μm sections, and collected on RNase-free polyethylene naphthalate membrane slides (Leica). Sections were stained with 0.1% toluidine blue, dehydrated with both 50 and 75% ethanol, and air dried. ONL was microdissected on a LCM system (LMD-7000; Leica).

Measurement of mRNA expression by real-time PCR. Whole retina or ONL dissected by LCM were used for PCR. Total RNA was harvested using the RNeasy Kit (Qiagen, Valencia, CA, USA). cDNA was generated with Oligo-dT primer (Invitrogen) and Superscript II (Invitrogen) according to the manufacturer's instructions. Real-time PCR was carried out using the following TaqMan gene expression assays (Applied Biosystems, Foster City, CA, USA): MST1 (Mm00451755_m1), MST2 (Mm01168119_m1), PUMA (Mm00519268_m1), Fas (Mm01204974_m1), actin (Mm00607939_s1). Quantitative expression data were acquired and analyzed with a Step One Plus real-time PCR system (Applied Biosystems).

ELISA. The levels of MCP-1 and IL-6 were determined with mouse MCP-1 and IL-6 ELISA kits (R&D Systems, Minneapolis, MN, USA), according to the manufacturer's protocol.

Immunohistochemistry. Sections were fixed in acetone for 5 min, blocked in 2% skim milk for 20 min, and incubated with rat anti-CD11b antibody (1:50; BD Biosciences) at 4 °C overnight. Alexa Fluor 488-conjugated goat anti-rat IgG was used as a secondary antibody and incubated at room temperature for 30 min. Finally, sections were counterstained with TO-PRO-3.

Statistical analysis. The results are expressed as the mean ± SE. Statistical analysis was performed nonparametrically with Mann–Whitney *U*-test. The significance level was set at $P<0.05$ (* in figures) and $P<0.01$ (** in figures). Statistical analysis and graphing were performed using Prism Ver.5.

Conflict of Interest

The authors declare no conflict of interest.

Acknowledgements. This work was supported by Foundation Lions Eye Research Fund (DGV); The Yeatts Family Foundation (DGV, JWM); 2013 Macula Society Research Grant award (DGV); Bausch & Lomb Vitreoretinal Fellowship (HM); a Special Scholar Award (KMC), a Physician Scientist Award (DGV) and unrestricted grant (JWM) from the Research to Prevent Blindness Foundation; NEI R21EY023079-01/A1 (DGV), NIH R01EY022084–01/S1 (KMC) and NEI grant EY014104 (MEEI Core Grant). The content is solely the responsibility of the authors and does not necessarily represent the official views of the National Eye Institute or the National Institutes of Health.

1. Trichonas G, Murakami Y, Thanos A, Morizane Y, Kayama M, Debouck CM *et al.* Receptor interacting protein kinases mediate retinal detachment-induced photoreceptor necrosis and compensate for inhibition of apoptosis. *Proc Natl Acad Sci USA* 2010; **107**: 21695–21700.
2. Zacks DN, Zheng QD, Han Y, Bakhru R, Miller JW. FAS-mediated apoptosis and its relation to intrinsic pathway activation in an experimental model of retinal detachment. *Invest Ophthalmol Vis Sci* 2004; **45**: 4563–4569.
3. Zacks DN, Boehlke C, Richards AL, Zheng QD. Role of the Fas-signaling pathway in photoreceptor neuroprotection. *Arch Ophthalmol* 2007; **125**: 1389–1395.
4. Besirli CG, Chinskey ND, Zheng QD, Zacks DN. Inhibition of retinal detachment-induced apoptosis in photoreceptors by a small peptide inhibitor of the fas receptor. *Invest Ophthalmol Vis Sci* 2010; **51**: 2177–2184.
5. Dunaief JL, Dentchev T, Ying GS, Milam AH. The role of apoptosis in age-related macular degeneration. *Arch Ophthalmol* 2002; **120**: 1435–1442.
6. Barber AJ, Lieth E, Khin SA, Antonetti DA, Buchanan AG, Gardner TW. Neural apoptosis in the retina during experimental and human diabetes. Early onset and effect of insulin. *J Clin Invest* 1998; **102**: 783–791.
7. Hellstrom A, Smith LE, Dammann O. Retinopathy of prematurity. *Lancet* 2013; **382**: 1445–1457.
8. Mitry D, Fleck BW, Wright AF, Campbell H, Charteris DG. Pathogenesis of rhegmatogenous retinal detachment: predisposing anatomy and cell biology. *Retina* 2010; **30**: 1561–1572.
9. Arroyo JG, Yang L, Bula D, Chen DF. Photoreceptor apoptosis in human retinal detachment. *Am J Ophthalmol* 2005; **139**: 605–610.
10. Campo RV, Sipperley JO, Sneed SR, Park DW, Dugel PU, Jacobsen J *et al.* Pars plana vitrectomy without scleral buckle for pseudophakic retinal detachments. *Ophthalmology* 1999; **106**: 1811–1815; discussion 1816.
11. Harvey KF, Pfleger CM, Hariharan IK. The *Drosophila* Mst ortholog, hippo, restricts growth and cell proliferation and promotes apoptosis. *Cell* 2003; **114**: 457–467.
12. Pan D. Hippo signaling in organ size control. *Genes Dev* 2007; **21**: 886–897.
13. Zeng Q, Hong W. The emerging role of the hippo pathway in cell contact inhibition, organ size control, and cancer development in mammals. *Cancer Cell* 2008; **13**: 188–192.
14. Kango-Singh M, Singh A. Regulation of organ size: insights from the *Drosophila* Hippo signaling pathway. *Dev Dyn* 2009; **238**: 1627–1637.
15. Zhao B, Li L, Lei Q, Guan KL. The Hippo-YAP pathway in organ size control and tumorigenesis: an updated version. *Genes Dev* 2010; **24**: 862–874.
16. Avruch J, Zhou D, Fitamant J, Bardeesy N. Mst1/2 signalling to Yap: gatekeeper for liver size and tumour development. *Br J Cancer* 2011; **104**: 24–32.
17. Zhao B, Wei X, Li W, Udan RS, Yang Q, Kim J *et al.* Inactivation of YAP oncoprotein by the Hippo pathway is involved in cell contact inhibition and tissue growth control. *Genes Dev* 2007; **21**: 2747–2761.
18. Hao Y, Chun A, Cheung K, Rashidi B, Yang X. Tumor suppressor LATS1 is a negative regulator of oncogene YAP. *J Biol Chem* 2008; **283**: 5496–5509.
19. Zhang J, Smolen GA, Haber DA. Negative regulation of YAP by LATS1 underscores evolutionary conservation of the *Drosophila* Hippo pathway. *Cancer Res* 2008; **68**: 2789–2794.
20. Vassilev A, Kaneko KJ, Shu H, Zhao Y, DePamphilis ML. TEAD/TEF transcription factors utilize the activation domain of YAP65, a Src/Yes-associated protein localized in the cytoplasm. *Genes Dev* 2001; **15**: 1229–1241.
21. Zhao B, Ye X, Yu J, Li L, Li W, Li S *et al.* TEAD mediates YAP-dependent gene induction and growth control. *Genes Dev* 2008; **22**: 1962–1971.
22. Zender L, Spector MS, Xue W, Flemming P, Cordon-Cardo C, Silke J *et al.* Identification and validation of oncogenes in liver cancer using an integrative oncogenomic approach. *Cell* 2006; **125**: 1253–1267.
23. Overholtzer M, Zhang J, Smolen GA, Muir B, Li W, Sgroi DC *et al.* Transforming properties of YAP, a candidate oncogene on the chromosome 11q22 amplicon. *Proc Natl Acad Sci USA* 2006; **103**: 12405–12410.
24. Zhou D, Conrad C, Xia F, Park JS, Payer B, Yin Y *et al.* Mst1 and Mst2 maintain hepatocyte quiescence and suppress hepatocellular carcinoma development through inactivation of the Yap1 oncogene. *Cancer Cell* 2009; **16**: 425–438.
25. Song H, Mak KK, Topol L, Yun K, Hu J, Garrett L *et al.* Mammalian Mst1 and Mst2 kinases play essential roles in organ size control and tumor suppression. *Proc Natl Acad Sci USA* 2010; **107**: 1431–1436.
26. Lu L, Li Y, Kim SM, Bossuyt W, Liu P, Qiu Q *et al.* Hippo signaling is a potent *in vivo* growth and tumor suppressor pathway in the mammalian liver. *Proc Natl Acad Sci USA* 2010; **107**: 1437–1442.
27. Strano S, Monti O, Pediconi N, Baccarini A, Fontemaggi G, Lapi E *et al.* The transcriptional coactivator Yes-associated protein drives p73 gene-target specificity in response to DNA Damage. *Mol Cell* 2005; **18**: 447–459.
28. Matallanas D, Romano D, Yee K, Meissl K, Kucerova L, Piazzolla D *et al.* RASSF1A elicits apoptosis through an MST2 pathway directing proapoptotic transcription by the p73 tumor suppressor protein. *Mol Cell* 2007; **27**: 962–975.
29. Lapi E, Di Agostino S, Donzelli S, Gal H, Domany E, Rechavi G *et al.* PML, YAP, and p73 are components of a proapoptotic autoregulatory feedback loop. *Mol Cell* 2008; **32**: 803–814.
30. Downward J, Basu S. YAP and p73: a complex affair. *Mol Cell* 2008; **32**: 749–750.
31. Romano D, Matallanas D, Weitsman G, Preisinger C, Ng T, Kolch W. Proapoptotic kinase MST2 coordinates signaling crosstalk between RASSF1A, Raf-1, and Akt. *Cancer Res* 2010; **70**: 1195–1203.
32. Khokhlatchev A, Rabizadeh S, Xavier R, Nedwidek M, Chen T, Zhang XF *et al.* Identification of a novel Ras-regulated proapoptotic pathway. *Curr Biol* 2002; **12**: 253–265.
33. Praskova M, Khoklatchev A, Ortiz-Vega S, Avruch J. Regulation of the MST1 kinase by autophosphorylation, by the growth inhibitory proteins, RASSF1 and NORE1, and by Ras. *Biochem J* 2004; **381**: 453–462.
34. Lehtinen MK, Yuan Z, Boag PR, Yang Y, Villen J, Becker EB *et al.* A conserved MST-FOXO signaling pathway mediates oxidative-stress responses and extends life span. *Cell* 2006; **125**: 987–1001.
35. Yuan Z, Lehtinen MK, Merlo P, Villen J, Gygi S, Bonni A. Regulation of neuronal cell death by MST1-FOXO1 signaling. *J Biol Chem* 2009; **284**: 11285–11292.
36. Liu W, Wu J, Xiao L, Bai Y, Qu A, Zheng Z *et al.* Regulation of neuronal cell death by c-Abl-Hippo/MST2 signaling pathway. *PLoS One* 2012; **7**: e36562.
37. Lee JK, Shin JH, Hwang SG, Gwag BJ, McKee AC, Lee J *et al.* MST1 functions as a key modulator of neurodegeneration in a mouse model of ALS. *Proc Natl Acad Sci USA* 2013; **110**: 12066–12071.
38. Matsumoto H, Miller JW, Vavvas DG. Retinal detachment model in rodents by subretinal injection of sodium hyaluronate. *J Vis Exp* 2013; (79): doi:10.3791/50660.
39. Melino G, Bernassola F, Ranalli M, Yee K, Zong WX, Corazzari M *et al.* p73 Induces apoptosis via PUMA transactivation and Bax mitochondrial translocation. *J Biol Chem* 2004; **279**: 8076–8083.
40. Schilling T, Schleithoff ES, Kairat A, Melino G, Stremmel W, Oren M *et al.* Active transcription of the human FAS/CD95/TNFRSF6 gene involves the p53 family. *Biochem Biophys Res Commun* 2009; **387**: 399–404.

41. Da CL, Xin Y, Zhao J, Luo XD. Significance and relationship between Yes-associated protein and survivin expression in gastric carcinoma and precancerous lesions. *World J Gastroenterol* 2009; **15**: 4055–4061.
42. Avruch J, Zhou D, Bardeesy N. YAP oncogene overexpression supercharges colon cancer proliferation. *Cell Cycle* 2012; **11**: 1090–1096.
43. Nakazawa T, Hisatomi T, Nakazawa C, Noda K, Maruyama K, She H *et al.* Monocyte chemoattractant protein 1 mediates retinal detachment-induced photoreceptor apoptosis. *Proc Natl Acad Sci USA* 2007; **104**: 2425–2430.
44. Zacks DN, Han Y, Zeng Y, Swaroop A. Activation of signaling pathways and stress-response genes in an experimental model of retinal detachment. *Invest Ophthalmol Vis Sci* 2006; **47**: 1691–1695.
45. Fisher SK, Erickson PA, Lewis GP, Anderson DH. Intraretinal proliferation induced by retinal detachment. *Invest Ophthalmol Vis Sci* 1991; **32**: 1739–1748.
46. Fisher SK, Lewis GP, Linberg KA, Barawid E, Verardo MR. Cellular Remodeling in Mammalian Retina Induced by Retinal Detachment. In: Kolb H, Fernandez E, Nelson R (eds). *The Organization of the Retina and Visual System*. University of Utah Health Sciences Center: Salt Lake City (UT), 1995.
47. Lewis GP, Matsumoto B, Fisher SK. Changes in the organization and expression of cytoskeletal proteins during retinal degeneration induced by retinal detachment. *Invest Ophthalmol Vis Sci* 1995; **36**: 2404–2416.
48. Lewis GP, Sethi CS, Carter KM, Charteris DG, Fisher SK. Microglial cell activation following retinal detachment: a comparison between species. *Mol Vis* 2005; **11**: 491–500.
49. Sethi CS, Lewis GP, Fisher SK, Leitner WP, Mann DL, Luthert PJ *et al.* Glial remodeling and neural plasticity in human retinal detachment with proliferative vitreoretinopathy. *Invest Ophthalmol Vis Sci* 2005; **46**: 329–342.
50. Creasy CL, Chernoff J. Cloning and characterization of a member of the MST subfamily of Ste20-like kinases. *Gene* 1995; **167**: 303–306.
51. Kim D, Shu S, Coppola MD, Kaneko S, Yuan ZQ, Cheng JQ. Regulation of proapoptotic mammalian ste20-like kinase MST2 by the IGF1-Akt pathway. *PLoS One* 2010; **5**: e9616.
52. Zhou Y, Callendret B, Xu D, Brasky KM, Feng Z, Hensley LL *et al.* Dominance of the CD4(+) T helper cell response during acute resolving hepatitis A virus infection. *J Exp Med* 2012; **209**: 1481–1492.
53. O'Neill E, Rushworth L, Baccarini M, Kolch W. Role of the kinase MST2 in suppression of apoptosis by the proto-oncogene product Raf-1. *Science* 2004; **306**: 2267–2270.
54. Chen J, Fujii K, Zhang L, Roberts T, Fu H. Raf-1 promotes cell survival by antagonizing apoptosis signal-regulating kinase 1 through a MEK-ERK independent mechanism. *Proc Natl Acad Sci USA* 2001; **98**: 7783–7788.
55. Ehrenreiter K, Piazzolla D, Velamoor V, Sobczak I, Small JV, Takeda J *et al.* Raf-1 regulates Rho signaling and cell migration. *J Cell Biol* 2005; **168**: 955–964.
56. Niault T, Sobczak I, Meissl K, Weitsman G, Piazzolla D, Maurer G *et al.* From autoinhibition to inhibition in trans: the Raf-1 regulatory domain inhibits Rok-alpha kinase activity. *J Cell Biol* 2009; **187**: 335–342.
57. Roh MI, Murakami Y, Thanos A, Vavvas DG, Miller JW. Edaravone an ROS scavenger, ameliorates photoreceptor cell death after experimental retinal detachment. *Invest Ophthalmol Vis Sci* 2011; **52**: 3825–3831.
58. Mantopoulos D, Murakami Y, Comander J, Thanos A, Roh M, Miller JW *et al.* Tauroursodeoxycholic acid (TUDCA) protects photoreceptors from cell death after experimental retinal detachment. *PLoS One* 2011; **6**: e24245.
59. Mantovani A, Sozzani S, Locati M, Allavena P, Sica A. Macrophage polarization: tumor-associated macrophages as a paradigm for polarized M2 mononuclear phagocytes. *Trends Immunol* 2002; **23**: 549–555.
60. Gordon S, Martinez FO. Alternative activation of macrophages: mechanism and functions. *Immunity* 2010; **32**: 593–604.
61. Sica A, Mantovani A. Macrophage plasticity and polarization: *in vivo* veritas. *J Clin Invest* 2012; **122**: 787–795.
62. Murakami Y, Matsumoto H, Roh M, Suzuki J, Hisatomi T, Ikeda Y *et al.* Receptor interacting protein kinase mediates necrotic cone but not rod cell death in a mouse model of inherited degeneration. *Proc Natl Acad Sci USA* 2012; **109**: 14598–14603.
63. Cavassani KA, Ishii M, Wen H, Schaller MA, Lincoln PM, Lukacs NW *et al.* TLR3 is an endogenous sensor of tissue necrosis during acute inflammatory events. *J Exp Med* 2008; **205**: 2609–2621.
64. Xu J, Zhang X, Pelayo R, Monestier M, Ammollo CT, Semeraro F *et al.* Extracellular histones are major mediators of death in sepsis. *Nat Med* 2009; **15**: 1318–1321.
65. Murakami Y, Matsumoto H, Roh M, Giani A, Kataoka K, Morizane Y *et al.* Programmed necrosis, not apoptosis, is a key mediator of cell loss and DAMP-mediated inflammation in dsRNA-induced retinal degeneration. *Cell Death Differ* 2014; **21**: 270–277.
66. Taylor KR, Yamasaki K, Radek KA, Di Nardo A, Goodarzi H, Golenbock D *et al.* Recognition of hyaluronan released in sterile injury involves a unique receptor complex dependent on Toll-like receptor 4, CD44, and MD-2. *J Biol Chem* 2007; **282**: 18265–18275.
67. Midwood K, Sacre S, Piccinini AM, Inglis J, Trebaul A, Chan E *et al.* Tenascin-C is an endogenous activator of Toll-like receptor 4 that is essential for maintaining inflammation in arthritic joint disease. *Nat Med* 2009; **15**: 774–780.

Supplementary Information accompanies this paper on Cell Death and Disease website (http://www.nature.com/cddis)